

# A GENERAL FRAMEWORK FOR SUPPORTING ECONOMIC FEASIBILITY OF GENERATOR AND STORAGE ENERGY SYSTEMS THROUGH CAPACITY AND DISPATCH OPTIMIZATION

**Saeed Azad\***

Postdoctoral Fellow

Department of Systems Engineering  
Colorado State University  
Fort Collins, CO 80523

[saeed.azad@colostate.edu](mailto:saeed.azad@colostate.edu)

**Ziraddin Gulumjanli**

Graduate Student

Department of Systems Engineering  
Colorado State University  
Fort Collins, CO 80523

[ziraddin.gulumjanli@colostate.edu](mailto:ziraddin.gulumjanli@colostate.edu)

**Daniel R. Herber**

Assistant Professor

Department of Systems Engineering  
Colorado State University  
Fort Collins, CO 80523

[daniel.herber@colostate.edu](mailto:daniel.herber@colostate.edu)

## ABSTRACT

*Integration of various electricity-generating technologies (such as natural gas, wind, nuclear, etc.) with storage systems (such as thermal, battery electric, hydrogen, etc.) has the potential to improve the economic competitiveness of modern energy systems. Driven by the need to efficiently assess the economic feasibility of various energy system configurations in early system concept development, this work outlines a versatile computational framework for assessing the net present value of various integrated storage technologies. The subsystems' fundamental dynamics are defined, with a particular emphasis on balancing critical physical and economic domains to enable optimal decision-making in the context of capacity and dispatch optimization. In its presented form, the framework formulates a linear, convex optimization problem that can be efficiently solved using a direct transcription approach in the open-source software DTQP. Three case studies demonstrate and validate the framework's capabilities, highlighting its value and computational efficiency in facilitating the economic assessment of various energy system configurations. In particular, natural gas with thermal storage and carbon capture, wind energy with battery storage, and nuclear with hydrogen are demonstrated.*

**Keywords:** integrated energy systems, control co-design, generator & storage, capacity & dispatch, techno-economic analysis

## 1 INTRODUCTION

The ever-changing and increasing energy demand resulting from various technological advancements, such as renewable energy

and vehicle electrification, has significantly affected various aspects of the energy market, from energy supply networks to transportation, storage, and consumption. This increase in electricity demand coincides with environmental policies that dictate more stringent requirements on carbon emissions. Furthermore, the stability of the electrical grid and the profitability of energy producers will depend on more reliable and flexible production. To adapt to such policies while meeting the increasing energy demands of our society, a promising solution is the integration of various generation and storage systems [1]. This solution offers an integrated approach towards energy systems and is positioned to revolutionize the energy market economy [2].

This approach, which is closely related to *integrated energy systems* (IES) [1] and *hybrid energy systems* (HES) [3] offers an increase in flexibility and robustness of the energy supply/demand [4]. It also promotes new business models for some utility companies to better adapt to scientific, technological, political, and socio-economic developments. Since many utility companies are commercial units, their sustainable operation hinges on consistent generation of revenue. However, the combination of higher penetration of renewable energy sources, volatile fossil fuel prices, more stringent environmental policies, etc. can negatively affect the economic competitiveness of some technologies.

For example, the most expensive per unit electricity, which is typically produced by nuclear power (due to complexity, capital intensiveness, construction time, etc.), is purchased last during peak demand when other sources are not available. This, along with other factors such as costs of repair, has resulted in the retirement of over 12 nuclear power plants (NPP) from February 2013 through April 2021 [5]. The retirement of NPPs, which roughly produce a fifth of the total electricity generation and half

\*Corresponding author, [saeed.azad@colostate.edu](mailto:saeed.azad@colostate.edu)

of the non-fossil fuel-based electricity in the U.S. (with no intermittency), points to a changing energy landscape in which NPPs require flexibility in base load to remain competitive [6].

A potential solution is to increase the economic competitiveness of such technologies by configuring them as a part of integrated energy systems, operating simultaneously with other generators, functions such as carbon capture and storage (CCS), and energy storage units. For example, an NPP may supply power to the grid when electricity prices are high and store energy during periods of oversupply. Depending on the storage type, the stored energy can then be directly sold as electricity or in the form of another energy/commodity, such as thermal energy or hydrogen. The thermal energy can be directly sold to chemical plants for use in industrial processes, while hydrogen can be either combusted to generate additional electricity [7] or sold for use in fuel cells or the steel manufacturing industry.

To be economically beneficial, the flexibility added by incorporating these generators in the context of integrated energy systems must be sufficient to overcome the capital and operational cost of the technology over its lifetime. A techno-economic assessment, presented here as a net present value (NPV) objective, is often at the core of analyzing how the integration of new units (such as generator and storage) and functions (such as CCS, district heating/cooling, etc.) can affect the economy of the entire system. It is also central to any retrofit design efforts within a structured energy system.

To maximize NPV, storage capacities (i.e., plant variables) and requested power, charge, and discharge decisions (i.e., control variables) must be optimized within the context of capacity and dispatch optimization. This combination and consideration of design decisions are referred to as control co-design (CCD) [8]. This class of problems has been explored in the context of integrated energy systems for a natural gas combined cycle (NGCC) with thermal energy storage (TES) and CCS [9], light water reactor (LWR) with various TES technologies [6], and nuclear power plant with hydrogen production [10].

The resulting dynamic optimization problem, when used with high-fidelity, non-linear technical models, is often computationally expensive. For example, to reduce the computational cost, instead of solving the problem for an entire year, Ref. [11] considered a 24-hour horizon and solved the problem 365 times. For effective early-stage decision-making, ideally, only a few assumptions and adjustments need to be added beyond the core techno-economic ones needed for assessment. Therefore, there is a need for an efficient and versatile computational framework that can capture subsystems' basic dynamics, constraints, and NPV economic analysis to assess various system configurations and scenarios for integrated generator and storage energy systems.

This computational framework is further motivated by the fact that feasibility studies of various system configurations/architectures are often required before selecting the most prof-

itable option. Accounting for subsystems' basic dynamics offers flexibility in assessing different system architectures without spending an unreasonable amount of resources on the development, construction, and optimization of high-fidelity models. Given that specific system components, characteristics, and performance criteria are often unknown in early-stage design and will be determined in later steps, the balance of fidelity maintained in the proposed framework enables the evaluation of overall system performance without the need for the determination of specific subsystems and components. Finally, a versatile framework should assist in navigating the decision-making process among engineers with technical expertise in the field and those with limited backgrounds, such as stakeholders and investors, who are often among the primary decision-makers in the space.

Therefore, this article presents the development and demonstration of an open-source framework in MATLAB for assessing the *economic feasibility of generator and storage systems through CCD*, which we refer to as ECOGEN-CCD. Empowered by subsystems' basic dynamics, ECOGEN-CCD formulates the capacity & dispatch dynamic optimization problem that can be efficiently implemented and solved using the open-source MATLAB software DTQP [12, 13], which uses direct transcription with an automated optimization problem generation for linear-quadratic dynamic optimization problems. This improvement in efficiency is highlighted by the fact that ECOGEN-CCD, in its current form, is capable of solving a capacity and dispatch dynamic optimization problem with an hourly mesh for 30 years in less than 280 [s]. Compared with the tools utilized in Refs. [14] and [5], ECOGEN-CCD emphasizes the design and operation of an individual plant, consisting of a collection of generators, storage units, and functions. ECOGEN-CCD is an open-source tool that is made publicly available in Ref. [15].

The remainder of the article is organized in the following manner: Sec. 2 starts by describing some motivations for the proposed framework and then discusses framework architecture, problem elements, techno-economic considerations, and problem formulation; Sec. 3 is focused on the demonstration of the proposed framework using three case studies with different generator and storage technologies, including an NGCC with TES and CCS, wind energy with battery energy storage, and an NPP with hydrogen generation and storage; and Sec. 4 offers some remarks regarding conclusions, limitations, and future directions.

## 2 PROBLEM DESCRIPTION

In this section, we describe the IES architecture, problem elements, techno-economic considerations, and the capacity and dispatch optimization problem.

### 2.1 IES Architecture

Figure 1 describes the general architecture of an integrated energy system (IES) considered in this framework. An IES is char-

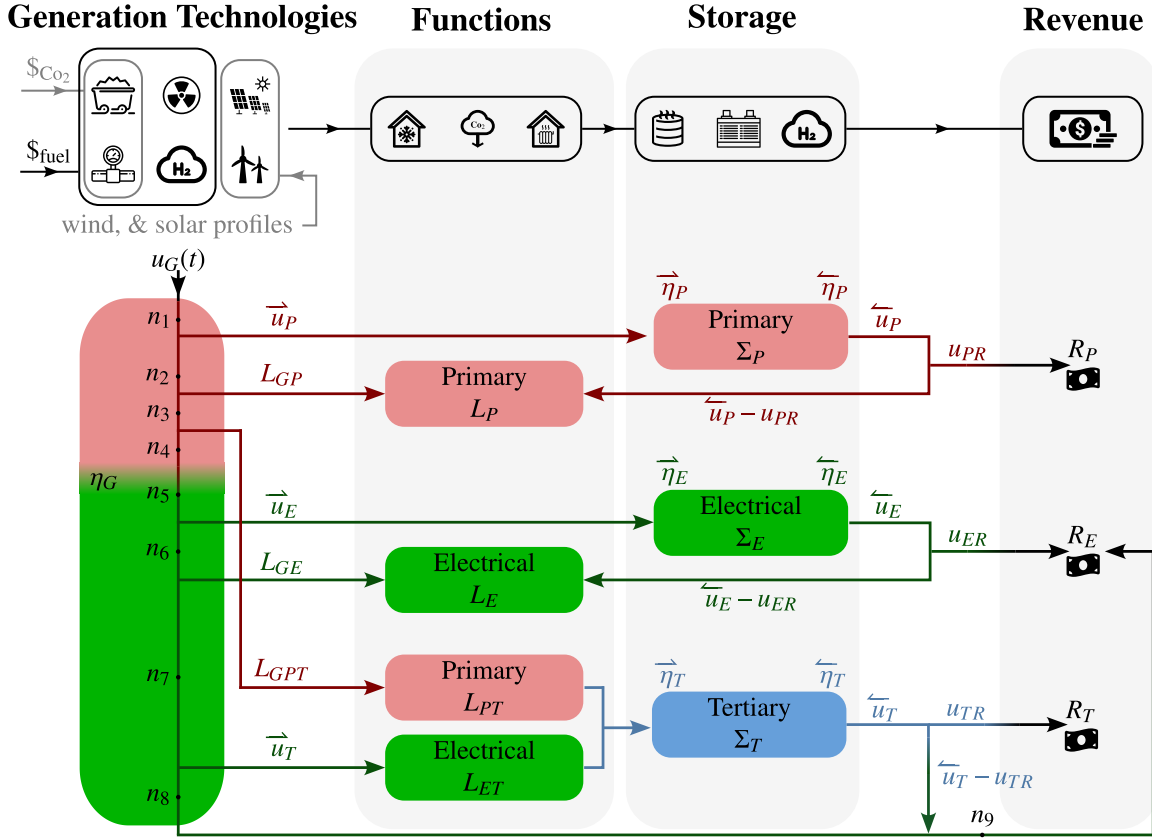


**FIGURE 1:** Illustration of an IES architecture with a collection of homogeneous electric power generators and three types of storage systems. Primary (such as thermal), electrical (such as battery), and tertiary (such as hydrogen) storage is shown in red, green, and blue, respectively. The charge and discharge signals, along with their associated efficiencies, are described by  $\vec{\bullet}$  and  $\overleftarrow{\bullet}$ , respectively.

acterized by various generators (e.g., NGCC power plant, wind farm, or NPP) and storage units (e.g., TES, battery energy storage system (BESS), or hydrogen storage). Additional functions (e.g., CCS, district heating/cooling, etc.) may also be present in the system and are characterized by the addition of their associated costs and energy requirements.

The generator, which is described by the subscript  $\bullet_G$ , is the unit responsible for producing electricity from an energy vector (e.g., natural gas) by often converting it first to a primary energy domain (e.g., thermal energy), and ultimately converting it to electricity with efficiency of  $\eta_G$ :

$$\text{generator's primary energy domain} \xrightarrow{\eta_G} \text{electricity} \quad (1)$$

Based on the desired configuration, the generator may have access to three different types of storage systems, distinguished through the subscript  $\bullet_S$ . These storage systems are defined based on their key energy domain. The first storage system uses the generator's primary domain,  $\bullet_P$ , to store energy. As an example, in an NGCC power plant, the primary energy domain is thermal energy. Thus, the primary storage system for this gener-

ator is a TES unit. In this work, the secondary energy domain is always electrical,  $\bullet_E$ . Therefore, the second storage type directly stores energy as electricity (e.g., through a BESS). A third storage facility,  $\bullet_T$ , is included to enable the usage of electricity to create a new product, commodity, service, or energy storage in a distinct medium, such as hydrogen.

The storage system is characterized by charge  $\vec{\bullet}$  and discharge  $\overleftarrow{\bullet}$  signals (noting the arrow directions). The charge signal can be affected by losses during the transmission. Therefore, its efficiency is denoted by  $\vec{\eta}_\bullet$ . The output efficiency of the storage is described as  $\overleftarrow{\eta}_\bullet$ :

$$\text{charging signal} \xrightarrow{\vec{\eta}_\bullet} \text{storage} \quad (2a)$$

$$\text{storage} \xrightarrow{\overleftarrow{\eta}_\bullet} \text{discharge signal} \quad (2b)$$

This systematic separation of efficiencies allows us, in the future, to consider additional factors, such as the distance between the facilities, that can affect the efficiency of energy transmission. An additional revenue-driven control signal, represented by  $\bullet_R$ , is responsible for deciding the percentage of the

discharge signal that is immediately turned into revenue through direct sales. For example, the revenue signal will decide how much of the discharged hydrogen is sold at current hydrogen prices. The remaining product will be combusted and sold as electricity.

The inclusion of various functions may result in the presence of additional load requirements. For example, in addition to auxiliary electrical loads, the operation of a CCS unit, which is assumed to be in operation whenever the generator is on, requires additional thermal and electrical loads. These loads are a function of the generator's current power level, presented as a certain percentage of the power plant's power level. Similarly, a high-temperature steam electrolysis (HTSE) process in a hydrogen plant (tertiary storage) requires both thermal and electrical energy. However, these load requirements are active only when a decision is made to generate hydrogen from the excess electricity. Therefore, these loads are a function of the tertiary charging signal, presented as a certain percentage of its current value.

The top part of Fig. 1 highlights some considerations regarding the electric energy technologies, including fuel cost, carbon tax, and dispatchable versus non-dispatchable type of resources. The bottom part presents a case for a collection of homogeneous generators (e.g., a wind farm) in the presence of multiple functions and storage types. The nodes in this figure, which are described by  $n_1, \dots, n_9$  are used to formulate some of the necessary constraints within the optimization problem and are mathematically described in Appendix A.

## 2.2 Problem Elements

This section introduces some problem elements based on the comprehensive case in which a collection of homogeneous generators have potential access to all 3 storage types in the presence of both primary and electrical loads. Adding the capability of simultaneously working with multiple non-homogeneous generators will be a future step of this work. Similarly, in the future, we plan to enable a more advanced integration of storage units in the toolbox, such that multiple storage topologies (e.g., two battery storage and one hydrogen storage) can be simultaneously integrated with ECOGEN-CCD.

**Plant Variables:** The capacity of each storage type is a sizing decision that will be determined by the optimizer and constitutes the plant optimization variables  $\Sigma$ :

$$\Sigma = [\Sigma_P, \Sigma_E, \Sigma_T]^T \quad (3)$$

Note that the vector of plant optimization variables reduces in size if the study does not include all three storage types.

**Control Variables:** Every energy storage system entails 3 control variables, one for charging the storage ( $\vec{u}_*$ ), one for discharging the storage  $\vec{u}_*$ , and one for determining the fraction of discharge  $u_{*R}$  that is directly used to generate revenue without any intermediate steps. In addition, the operator can request a

specific power from the generator through a control command, described as  $u_G(t)$ . The vector of control variables can then be defined as:

$$\begin{aligned} \mathbf{u}(t) &= [u_G(t), \mathbf{u}_S(t)]^T \\ &= [u_G(t), \mathbf{u}_{SP}(t), \mathbf{u}_{SE}(t), \mathbf{u}_{ST}(t)]^T \end{aligned} \quad (4)$$

Here, every storage control vector  $\mathbf{u}_{S*}(t)$  consists of 3 variables  $\mathbf{u}_{S*}(t) = [\vec{u}_*(t), \vec{u}_*(t), u_{*R}(t)]^T$ . Similar to the previous case, the size of the control vector will be reduced if only some of the storage types are included in the study.

**State Variables:** There is one state variable associated with the generator which describes the power level of the generator using a ramp rate of  $\tau$ :

$$\dot{x}_G(t) = \frac{1}{\tau}(-x_G(t) + u_G(t)) \quad (5)$$

Each storage system is characterized by a state variable that describes the current amount of stored energy in that system. For the most comprehensive case with 3 different storage facilities, the storage dynamics are described by:

$$\dot{\mathbf{x}}_S(t) = \begin{bmatrix} \dot{x}_P(t) \\ \dot{x}_E(t) \\ \dot{x}_T(t) \end{bmatrix} = \begin{bmatrix} \overbrace{\vec{\eta}_P \vec{u}_P(t)}^{\text{Charge}} \\ \overbrace{\vec{\eta}_E \vec{u}_E(t)}^{\text{Charge}} \\ \overbrace{\alpha_{ET} \vec{\eta}_T \vec{u}_T(t)}^{\text{Discharge}} \end{bmatrix} - \begin{bmatrix} \vec{u}_P(t) \\ \vec{u}_E(t) \\ \vec{u}_T(t) \end{bmatrix} \quad (6)$$

where  $\alpha_{ET}$  is the conversion rate between electricity and the tertiary commodity. Describing storage states in vector form and augmenting them with generator state, the dynamics of the problem are described by:

$$\begin{aligned} \dot{\mathbf{x}}(t) &= \mathbf{A}\mathbf{x}(t) + \mathbf{B}\mathbf{u}(t) \\ \begin{bmatrix} \dot{x}_G(t) \\ \dot{\mathbf{x}}_S(t) \end{bmatrix} &= \begin{bmatrix} -1/\tau & \mathbf{0} \\ \mathbf{0} & \mathbf{0} \end{bmatrix} \begin{bmatrix} x_G(t) \\ \mathbf{x}_S(t) \end{bmatrix} + \begin{bmatrix} 1/\tau & \mathbf{0} \\ \mathbf{0} & \mathbf{b}_S \end{bmatrix} \begin{bmatrix} u_G(t) \\ \mathbf{u}_S(t) \end{bmatrix} \end{aligned} \quad (7)$$

where  $\mathbf{b}_S$  is the appropriately-sized matrix:

$$\mathbf{b}_S = \begin{bmatrix} \vec{\eta}_P & -1 & 0 & 0 & 0 & 0 & 0 & 0 & 0 \\ 0 & 0 & 0 & \vec{\eta}_E & -1 & 0 & 0 & 0 & 0 \\ 0 & 0 & 0 & 0 & 0 & 0 & \alpha_{ET} \vec{\eta}_T & -1 & 0 \end{bmatrix} \quad (8)$$

**Constraints:** This section presents all of the time-independent and time-dependent constraints in the dynamic optimization problem.

The storage capacities are non-negative. Therefore, the following constraint is imposed on plant variables:

$$\mathbf{0} \leq \Sigma \quad (9)$$

The requested power from the generator is non-negative and less or equal to the net nominal capacity of the generator. Similarly, the charge and discharge signals are non-negative and never greater than the maximum energy transfer rate into and out of the storage system, respectively. These maximum and minimum energy transfer rates are currently input parameters but will be added to the set of potential plant optimization variables in the

future, similar to Ref. [9]. These constraints are succinctly described in vector form as:

$$\mathbf{0} \leq \mathbf{u}(t) \leq \mathbf{u}_{\max}(t) \quad (10a)$$

Specifically, the revenue-generating fraction of the control signal in Eq. (10) is non-negative and equal to or smaller than the discharge signal:

$$u_{PR}(t) \leq \bar{u}_P(t) \quad (10b)$$

$$u_{ER}(t) \leq \bar{u}_E(t) \quad (10c)$$

$$u_{TR}(t) \leq \bar{u}_T(t) \quad (10d)$$

The generator's power level must remain non-negative and never exceed its nominal capacity. Requesting a specific (admissible) power output from the generator is reasonable for technologies such as nuclear or NGCC under simplifying assumptions like no temperature dependence on its operation or maintenance schedules. For intermittent technologies, such as wind and solar, they are at the mercy of the availability of (renewable) resources. In other words, the electricity produced by such technologies is not dispatchable due to the resource's inherent intermittency. Thus, it is necessary to ensure that the generator state  $x_G(t)$  is bounded by an input signal that represents the level of resource availability. These result in the following constraint on the generator's state:

$$x_{G,\min}(t) \leq x_G(t) \leq x_{G,\max}(t) \quad (11)$$

where  $x_G(t)$  refers to the generator's state, and  $x_{G,\max}(t)$  is an upper bound that is established based on nominal capacity, or the availability of renewable resources. Further details regarding the construction of  $x_{G,\max}(t)$  for a wind farm are included in Sec. 3.2.

The amount of stored energy must be non-negative and less or equal to the capacity of the storage system:

$$\mathbf{0} \leq x_S(t) \leq \Sigma \quad (12)$$

which represents a key coupling between select states and the plant parameters.

The initial states are prescribed for all the state variables. It is also assumed that at the final time  $t_f$ , the storage system has the same amount of stored energy at  $t_0$ :

$$x(t_0) = x_0 \quad (13a)$$

$$x_S(t_f) = x_S(t_0) \quad (13b)$$

where the latter equation is optional as multiple shorter, sequential time horizons do not necessitate this assumption [9].

In addition to the upper bound imposed by the maximum energy transfer rate for charging the storage system (Eq. 10), it is necessary to ensure that the charging signal is smaller or equal to the available power in the generator. This is described with the help of nodes that are placed in Fig. 1:

$$\bar{u}_P(t) \leq n_1(t) \quad (14a)$$

$$\bar{u}_E(t) \leq n_5(t) \quad (14b)$$

$$\bar{u}_T(t) \leq n_7(t) \quad (14c)$$

where the mathematical expressions associated with all of the nodes  $n_1, \dots, n_9$  are provided in Appendix A.

In addition, the generator's load-satisfying signals  $L_{GP}$ ,  $L_{GE}$ , and  $L_{PT}$  are non-negative. This condition is to ensure that power does not flow from the storage system into the generator. These signals are also upper-bounded by the available power in the generator. These constraints are formulated as:

$$\mathbf{0} \leq L_{GP}(t) \leq n_2(t) \quad (15a)$$

$$\mathbf{0} \leq L_{GPT}(t) \leq n_3(t) \quad (15b)$$

$$\mathbf{0} \leq L_{GE}(t) \leq n_5(t) \quad (15c)$$

**Objective Function:** The net present value (NPV) objective function, which enables the assessment of the economic viability of a given technology, is used in this framework. NPV is calculated as:

$$\text{maximize NPV} = -C_{\text{cap}}(\Sigma) + \int_{t_0}^{t_f} \frac{v_{\text{profit}}(\mathbf{u}, \mathbf{x}, \Sigma, t)}{D(t)} dt \quad (16)$$

where  $C_{\text{cap}}$  are the capital expenses,  $v_{\text{profit}}(t)$  is calculated as a function of expenses and revenues, and  $D(t)$  is the discounting function (money is 'worth' more now than in the future). An annualized discounting function is considered here as:

$$D(t) = (1 + r)^{\text{year}(t)} \quad (17)$$

where  $r$  is the discount rate and  $\text{year}(t)$  is the integer number of years that have passed since  $t_0$ . These intermediate quantities are now discussed in detail.

## 2.3 Techno-Economic Considerations

In order to construct the NPV objective function in Eq. (16), we first consider the sources of costs and revenues. These cost parameters are a user-defined input to the ECOGEN-CCD framework.

**2.3.1 Expenses** All of the costs included in the techno-economic analysis (including capital costs, fixed and variable operation and maintenance, fuel costs, and carbon costs) are described in this section.

**Capital Costs:** In this article, we assume that the capital cost,  $C_{\text{cap}}$  consists of overnight capital costs  $C_{\text{occ}}$ , and costs over the period of construction  $C_{cp}$ :

$$C_{\text{cap}} = C_{\text{occ}} + C_{cp} \quad (18)$$

where  $C_{\text{occ}}$  assumes that all of the construction occurs overnight. Therefore, this term excludes changes in the prices of goods and financial costs (such as the loan, inflation, discount rate, etc.). This allows potential investigations into the impact of construction periods, rates of inflation, etc. in the analysis [16].  $C_{\text{occ}}$  consists of direct construction costs, indirect construction costs, contingencies, and owner's cost, explained in detail in Ref. [17, 18].

$C_{cp}$  includes all the costs that are incurred over the construction period, such as escalation, loan, inflation, etc. Therefore,



this term is sensitive to the choice of financial parameters such as discount rate, debt-equity ratio, interest rate, interest during construction (IDC), etc. In this study, we simplify this term, similar to the methodology presented in Ref. [19], to account for the costs over the period of construction through a simple model characterizing IDC:

$$C_{\text{cap}} = C_{\text{occ}}(1 + C_{\text{idc}}) \quad (19)$$

where  $C_{\text{idc}}$  is calculated as a function of the construction time  $T_{\text{con}}$ , and the cost of capital rate  $r$ , estimated as:

$$C_{\text{idc}} = \frac{r}{2}T_{\text{con}} + \frac{r^2}{6}T_{\text{con}}^2 \quad (20)$$

Inclusion of more advanced financial parameters [9], such as loan, depreciation, etc. are future work items for this framework. For the entire system, the capital cost is expressed as:

$$C_{\text{cap}} = [C_{\text{occ}_G} + C_{\text{occ}_P}\Sigma_P + C_{\text{occ}_E}\Sigma_E + C_{\text{occ}_T}\Sigma_T](1 + C_{\text{idc}}) \quad (21)$$

**Operation and Maintenance (O&M):** The main elements included in O&M costs are associated with fixed and variable O&M costs. Fixed O&M costs, expressed as  $C_{\text{fom}}$ , include regular system maintenance, decommissioning, component replacement, etc. These costs only depend on the duration of the operation. For storage systems, these costs scale with storage size (e.g., more frequent and lengthier maintenance for larger capacities). Fixed O&M costs  $C_{\text{fom}}$  are then calculated as:

$$C_{\text{fom}}(t) = C_{\text{fom}_G} + C_{\text{fom}_P}\Sigma_P + C_{\text{fom}_E}\Sigma_E + C_{\text{fom}_T}\Sigma_T \quad (22)$$

Variable O&M costs, expressed as  $C_{\text{vom}}$ , reflect the non-fuel portion of the costs that vary by the amount of energy generated or supplied (such as water, waste disposal, lubricants, chemicals, and other consumable materials). Therefore, these costs depend on the power level of the unit, expressed as:

$$C_{\text{vom}}(t) = C_{\text{vom}_G}x_G(t) + C_{\text{vom}_P}(\vec{\eta}_P\vec{u}_P(t) + \overleftarrow{u}_P(t)) \quad (23a)$$

$$+ C_{\text{vom}_E}(\vec{\eta}_E\vec{u}_E(t) + \overleftarrow{u}_E(t)) \quad (23b)$$

$$+ C_{\text{vom}_T}(\alpha_{ET}\vec{\eta}_T\vec{u}_T(t) + \overleftarrow{u}_T(t)) \quad (23c)$$

**Fuel Costs:** Generally, fuel cycle cost,  $C_{\text{fuel}}(t)$  includes both front-end and back-end costs, such as supply, conversion, enrichment, fabrication, transportation, and waste disposal. For fossil fuels, the cost of fuel only entails the front-end costs, as received from the market. However, for nuclear power plants, the back-end costs are also included as a percentage of the front-end costs:

$$E_{\text{fuel}}(t) = \rho_{\text{fuel}}C_{\text{fuel}}(t)x_G(t) + B_{\text{fuel}}(t) \quad (24)$$

where  $\rho_{\text{fuel}}$  is the conversion factor between the power output of the generator and fuel consumed,  $C_{\text{fuel}}(t)$  is the instantaneous fuel prices, and  $B_{\text{fuel}}(t)$  is the back-end cost (again, mainly necessary for waste management and disposal in nuclear power plants).

**Carbon Cost:** With the goal of making the societal cost of carbon emissions visible, carbon cost, expressed as  $\text{CO}_2$ , assumes a carbon tax rate to incentivize clean electricity generation. The

cost of fuel is therefore estimated as:

$$E_{\text{CO}_2}(t) = C_{\text{CO}_2}\alpha_{\text{CO}_2}\rho_{\text{fuel}}x_G(t) \quad (25)$$

where  $C_{\text{CO}_2}$  is the carbon tax, and  $\alpha_{\text{CO}_2}$  is the amount of  $\text{CO}_2$  produced per unit of fuel.

**2.3.2 Revenue:** Here, the operator can earn revenue by either directly selling electricity to the grid (without using storage), or alternatively, using storage to sell primary energy, electricity, or a tertiary commodity. The total revenue is calculated for all energy domains as a function of their associated prices. The price arbitrage between primary, electricity, and tertiary domains determines the optimal flow of energy that maximizes the objective function. As an example, revenue earned by selling stored thermal energy to chemical plants (first term in Eq. (26)) is calculated as a function of thermal energy prices  $C_P(t)$ , discharge efficiency  $\vec{\eta}_P$ , and the revenue control signal  $u_{PR}(t)$ . However, the revenue control signal may only become active when the electricity prices are low and thermal energy prices are high. Note that for certain commodity types, such as hydrogen, it is also possible to generate electricity, which will then be sold to the grid. Mathematically, the revenue can be described as:

$$R = R_P(t) + R_E(t) + R_T(t) \quad (26)$$

$$\begin{aligned} &= C_P(t)\vec{\eta}_P u_{PR}(t) + C_E(t)\eta_G x_G(t) - C_E(t)\eta_G \vec{u}_P(t) \\ &\quad - C_E(t)\eta_G L_P x_G(t) + C_E(t)\eta_G \vec{\eta}_P \overleftarrow{u}_P(t) \\ &\quad - C_E(t)\eta_G \vec{\eta}_P u_{PR}(t) - C_E(t)\eta_G L_{PT} \vec{u}_T - C_E(t)\vec{u}_E(t) \\ &\quad - C_E(t)L_E x_G(t) + C_E(t)\vec{\eta}_E \vec{u}_E(t) - C_E(t)\vec{u}_T(t) \\ &\quad + \alpha_{TE}C_E(t)\vec{\eta}_T \overleftarrow{u}_T(t) - \alpha_{TE}C_E(t)\vec{\eta}_T u_{TR}(t) \\ &\quad + C_T(t)\vec{\eta}_T u_{TR}(t) \end{aligned}$$

where  $C_P(t)$  is the price of the primary energy,  $C_E(t)$  is the electricity price, and  $C_T(t)$  is the price of tertiary commodity/product.

## 2.4 Problem Formulation

With all of the problem elements defined, the economic feasibility of a candidate IES can be assessed through the optimization of capacity and dispatch within an all-at-one problem formulation:

$$\text{maximize: } \text{NPV}(t, \mathbf{u}, \mathbf{x}, \Sigma, \mathbf{d}) \quad (27a)$$

$$\text{subject to: } \mathbf{g}(t, \mathbf{u}, \mathbf{x}, \mathbf{p}, \mathbf{d}) \leq \mathbf{0} \quad (27b)$$

$$\dot{\mathbf{x}} - \mathbf{f}(t, \mathbf{u}, \mathbf{x}, \mathbf{p}, \mathbf{x}_0, \mathbf{d}) = \mathbf{0} \quad (27c)$$

$$\mathbf{x}(t_0) = \mathbf{x}_0 \quad (27d)$$

$$\mathbf{x}(t_f) = \mathbf{x}(t_0) \text{ (optional)} \quad (27e)$$

$$\text{where: } \mathbf{u} = \mathbf{u}(t), \mathbf{x} = \mathbf{x}(t) \quad (27f)$$

$$t \in [t_0, t_f], t_f = Nt_p \quad (27g)$$

where  $\mathbf{d}$  is the vector of problem parameters,  $\mathbf{g}(\cdot)$  is the vector of inequality constraints, associated with Eqs. (9)–(15c) and Eq. (27c) refers to systems dynamics described in Eqs. (5) and (6). Periodic conditions are defined in Eq. (27g) using a base pe-

riod  $t_p$ , and the number of repetitions,  $N$ . Periodic conditions can be adjusted by the user based on the availability of price signals, time horizon of the problem of interest, and other factors. For further clarification, this formulation is accompanied by Tab. 7, which provides a lexical interpretation for some of the problem elements. In addition, an optimization model presented in Fig. 14, is created in Sec. 5 to illustrate the relationship between various problem elements better.

As it is well established in mathematical optimization literature, the choice of units can negatively affect the problem's scaling and decrease its effectiveness [20]. Artfully changing the order of magnitude of problem elements can result in a more computationally-favorable problem, preventing unstable and inefficient algorithmic calculations [21]. As an example, solving the case studies in this article without appropriate scaling using  $10^{-6}$  solver tolerance can take up as much as a day of computational time. This is because the optimizer will spend a tremendous amount of time optimizing for  $10^{-6}$ th of a dollar value. From a broader perspective, it is clear that  $10^{-6}$ th of a dollar value is insignificant over the project's lifetime, which has an NPV value in the order of millions of dollars. Using a scaling factor of  $10^9$  for the objective function and appropriately-selected scaling factors for other problem elements, the problem can be solved in less than 280 seconds, signifying a dramatic increase in computational efficiency. Using the same solver tolerance of  $10^{-6}$ , the objective function will be optimal up to 99.9999% of the NPV value. A more comprehensive discussion on scaling in dynamic optimization problems is discussed in Ref. [21].

### 3 Case Studies

This section shows several case studies to demonstrate the capabilities of the proposed framework. These studies are selected to highlight, to the extent possible, different modes of operation using different technologies and storage types. Shared parameters among these technologies are described in Table 1.

ECOGEN-CCD uses an hourly time mesh within DTQP by default, although other time intervals (e.g., decisions being made every minute) can be used as desired. The control decisions over these intervals are piecewise constant, making the zero-order hold method suitable as it produces no discretization error for the state dynamics. The resulting capacity and dispatch optimization problem, with the current assumptions outlined in the previous section, is a linear optimization problem. Due to the problem's convexity property, it can be efficiently solved for the global optimal solution using MATLAB's quadprog optimization solver (although other solvers could be used given the problem matrices from DTQP). A solver tolerance of  $10^{-6}$  was used in quadprog, with an interior-point-convex algorithm to solve a dynamic optimization problem using direct transcription with an equidistant mesh and a composite Euler forward quadrature method.

Problem setup and solving times presented are associated with a single desktop workstation with an AMD Ryzen 9 3900X 12-core processor at 3.79 GHz, 32 GB of RAM, 64-bit Windows 10 Enterprise LTSC version 1809, and MatLab R2024a.

#### 3.1 Case Study I: Combined Cycle with Thermal Storage and Carbon Capture

To meet potential environmental requirements, fossil fuel-based generators, such as NGCC power plants, are considering a reduction in their carbon emissions through CCS functions. However, the inclusion of a CCS reduces the net plant efficiency and power output while increasing the cost of electricity [24]. A potential mitigating solution is to integrate the system with a thermal energy storage (TES), as discussed in detail in Refs. [9, 25].

This study assumes that the NGCC power plant, which is already built and equipped with a CCS unit (therefore, there is no overnight construction cost), is to be retrofitted to include a hot TES system. The CCS operates only when the plant is running. The CCS function is characterized by a thermal and electrical load, which are required for the operation of the CCS unit and are defined as a fixed percentage of the generator's power level. Therefore, whenever the generator is on, these electrical and thermal loads appear in the problem and must be satisfied. Including a hot thermal storage unit in the architecture enables operators to practically remove some of the parasitic thermal load from the power plant when the electricity prices are high, maximizing revenue. The considered system is illustrated in Fig. 2a, and specific, technology-dependent parameters are shown in Tab. 2.

The problem is carried out for 30 years of operation with an hourly time mesh (262980 time grid points), and it is assumed that thermal energy can not be directly sold; rather, it can only be used for meeting the thermal load demand from CCS. The input parameters associated with this case study, which are largely based on Refs. [9]–[22] and are tabulated in Tables 1 and 2. Due to linearity and convexity, a globally optimal solution is found efficiently in only 280 [s]. The results from this case study are discussed in the following and shown in Figs. 3 and 4.

The behavior of the candidate generator and storage system within the optimization problem is tightly associated with the cost of fuel and electricity. This study assumes that fuel prices are constant within each month. To understand the impact of the electricity price signal on the system's behaviors, we first interpret the results within a single month with fixed fuel prices. We have marked Fig. 3, with time periods ① and ②, which are associated with low and high electricity prices, respectively.

Accordingly, as shown in Fig. 3a, in the region marked by ①, electricity prices are low. Thus, operating the generator at full capacity is not profitable. However, this time window is a good opportunity for the generator to charge the storage, as shown in Fig. 3b. Figure 3c shows the charge and discharge signals during this period. Note that while both charging and discharging signals are active, the charging signal is larger, resulting in an in-

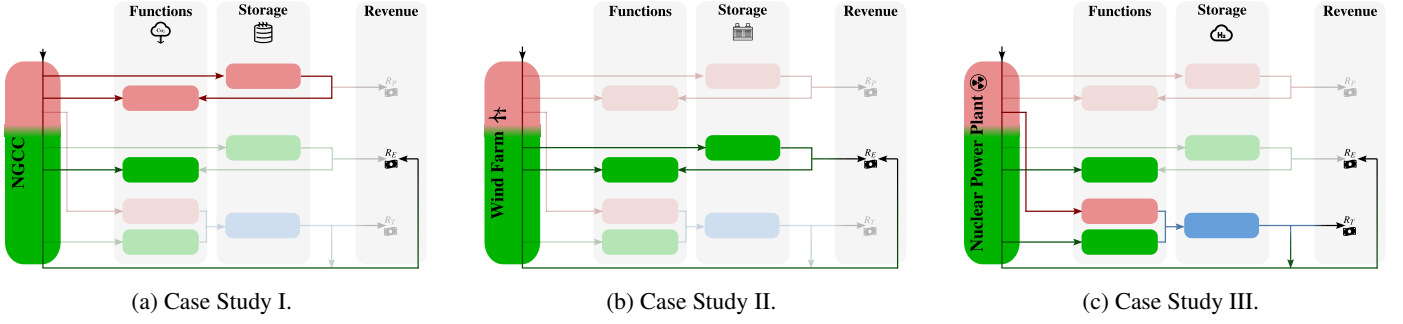


**FIGURE 2:** IES candidate for Case Study I: A natural gas combined cycle power plant with thermal storage and a carbon capture and storage system, Case Study II: A wind farm with a battery energy storage system, and Case Study III: A nuclear power plant with a hydrogen production (through high-temperature steam electrolysis) and storage facility.

**TABLE 1:** Cost parameters for generator and storage technologies used in Case Study I, II, and III.

Parameters	Generator				Storage				
	CC [22]	Wind [22]	Nuclear [22]	Unit	TES [9]	BESS [22]	Unit	Hydrogen [23]	Unit
Nom. cap.	1083	200	2156	MW	-	50	MW	640	tpd
$C_{occ}$	0	1265000	6041000	\$/MW	1048947	347000	\$/MWh	600.074	\$/kg
$C_{fom}$	12200	26340	121640	\$/MW-yr	4.7897	0.7178	\$/MWh-h	0	\$/kg-yr
$C_{vom}$	1.87	0	2.37	\$/MWh	0.75	0	\$/MWh	0.2884	\$/kg

**TABLE 2:** Parameters associated with Case Study I for combined cycle generator with CCS, and a thermal storage system largely based on Ref. [9].

Field	Value	Unit	Field	Value	Unit
$\rho_{fuel}$	146.952	kg/h.MW	$\alpha_{CO_2}$	0.0029	ton/kg
$\tau$	0.1389	h	$\eta_G$	1	-
$u_{G,min}$	0	MW	$u_{G,max}$	1083	MW
$x_{G,min}$	0	MW	$x_{G,max}$	1083	MW
$x_S(t_0)$	25	MWh	$x_G(t_f)$	25	MWh
$\bar{u}_{max}$	200	MW	$\bar{u}_{max}$	200	MW
$L_P$	$0.1x_G$	MW	$L_E$	$0.2x_G$	MW
$T_{con}$	3	years	$r$	0.075	-

crease in the storage state. During this period, the power sold to the grid is relatively lower than in other time periods, as shown in Fig. 3d.

The region marked by ② describes the system's response to a scenario in which the electricity prices are relatively high. During this period, it is profitable for the generator to run at full or high capacity (see Fig. 3a). According to Figs. 3b and 3c, high electricity prices also incentivize storage discharge during this period. The discharged thermal energy during this phase removes the dependent thermal load from the generator, allowing an increase in the amount of electricity sold to the grid. This is

shown in Fig. 3d.

To understand how the system behavior is affected by the combination of electricity and fuel prices, a longer horizon, during which both price signals change, is presented in Fig. 4. From this figure, it is clear that when the electricity prices are low and the fuel prices are high, the operation of the generator drops significantly to about 10% of its nominal capacity. This figure provides insights into the impact of fuel and electricity prices on the system's behavior, incentivizing the inclusion of future price increases (due to inflation, etc.) in our future work.

Overall, the optimal storage capacity is found to be 237.53 [MWh], and the NPV objective is  $\$ - 1.83 \times 10^9$ . Compared to the case with no thermal storage available (with CCS), this solution represents a 71.03% improvement in the project's economic viability. These results use several critical assumptions that should be reconsidered for evaluating a specific site location. Furthermore, current historical market signals were extrapolated from [26, 27], but including predicted future market signals (e.g., from Ref. [14, 28]) could aid in the decision making by considering the future grid composition and climate change. Even with these current assumptions, the expected trends are observed, and ECOGEN-CCD can be used as a strong framework for the early-stage investigation of these generator and storage technologies.

Assessing the share of various functions and requirements over the plant's lifetime can yield insights regarding its optimal operation. Specifically, Fig. 5 shows how the energy produced by



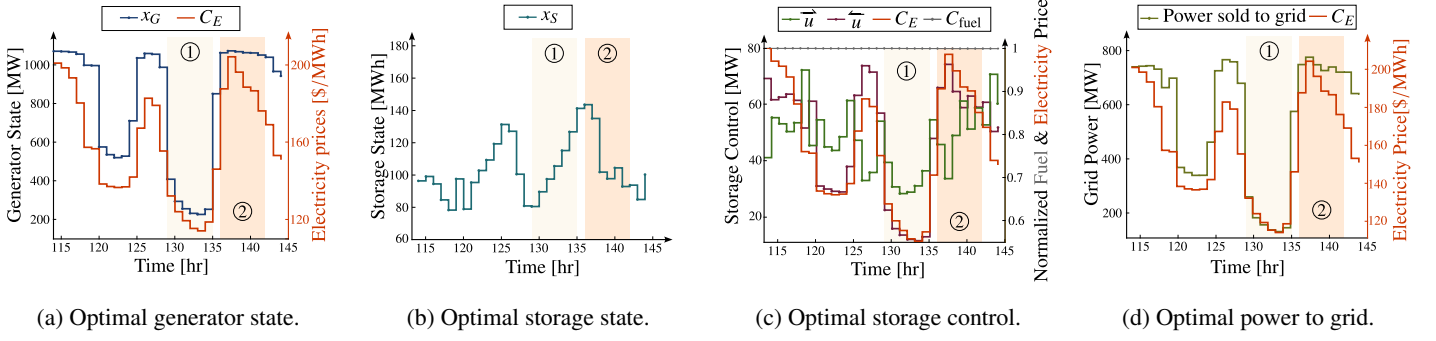


**FIGURE 3:** Case Study I: Optimal state and control variables for combined cycle generator with thermal storage and carbon capture.

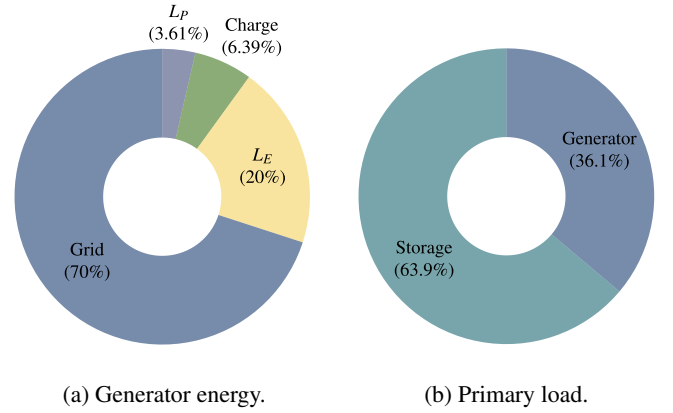
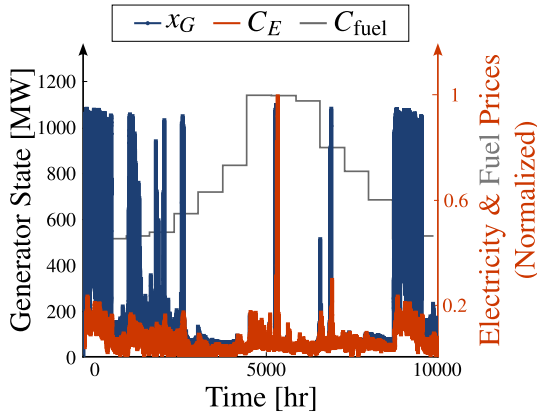


**FIGURE 4:** Case Study I: Optimal generator state with electricity and fuel prices over a long horizon of around 42 days.

the generator is utilized. Specifically, 70% of the generator energy is sold to the electricity grid, while 20%, 6.39%, and 3.61% are used for electric load, charge, and primary load, respectively. The relatively small share of the generator in satisfying the primary load is made possible through the inclusion of the thermal energy system, which is responsible for satisfying 63.9% of the thermal energy demand from CCS according to Fig. 5b. As shown in Fig. 5c, the storage system is responsible for about 9.09% of the overall revenue.

NGCC generators have traditionally served as peaking power plants, meaning that they are used during the peak electricity demand to satisfy the load. The requirement for following some electricity demand or the commitment to provide a certain amount of power to the grid during specific time periods has direct implications on optimal system behavior and storage sizing. To assess this impact, we consider the case in which the power plant is required to operate at its full capacity during peak hours  $T_{\text{peak}}$ . Moreover, since the generated power during this time period is committed to the electricity grid, no storage charging is

**FIGURE 5:** Breakdown of various elements in Case Study I, a combined cycle with thermal storage and carbon capture: (a) Generator energy usage, (b) Primary load contributions, and (c) Revenue contributions.

allowed. These considerations can be included in the optimization problem by updating some of the bounds in Eqs. (10a)–(11). The new operational constraints are mathematically formulated

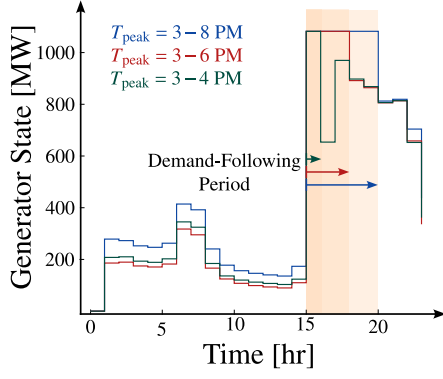


**FIGURE 6:** Generator state with demand-following constraints with 3 different demand-following periods.

as:

$$\vec{u}_{\max}(t) = \begin{cases} 0, & \text{if } t \in T_{\text{peak}} \\ \vec{u}_{\max}(t), & \text{otherwise} \end{cases} \quad (28)$$

$$x_{G,\min}(t) = \begin{cases} x_{G,\max}(t), & \text{if } t \in T_{\text{peak}} \\ 0, & \text{otherwise} \end{cases} \quad (29)$$

Assuming the daily peak power demand of  $T_{\text{peak}} = [3 - 7]$  PM, we solve the Case Study I in the presence of the demand-following constraint. As opposed to the previous case, where the generator would shut down or operate at a lower capacity when electricity prices were low and fuel costs were high, this case demonstrates a situation in which the NGCC power plant operates in a more restricted market. Compared to the previous case, the NGCC commitment to provide power to the grid regardless of electricity and fuel prices during the peak demand period negatively affects the economics of the plant, changing the NPV from  $\$ -1.83 \times 10^9$  to  $\$ -3.91 \times 10^9$ .

This scenario motivates more storage activity compared to the previous case. Specifically, since no charging is allowed during the peak demand, the overall charging activity is increased during non-peak hours when compared to the previous case. More extreme discharge activity is witnessed during the peak electricity demand, particularly during times when electricity prices are low and fuel costs are high. The discharge signal contributes to meeting the thermal load requirements for CCS operation, which is largest when the power plant is operating at its full capacity during peak demand hours. The important role of storage in this system is demonstrated by the 40.56% increase in optimal storage capacity from 237.53 [MWh] to 333.87 [MWh].

The sensitivity of the NPV objective function and storage capacity to the duration of the demand-following constraint is discussed next. Here, we perturb the duration of the demand-following constraint and examine the variations in optimal system behavior. Figure 6 presents the generator state in the presence of the demand-following constraint for 3 different demand-

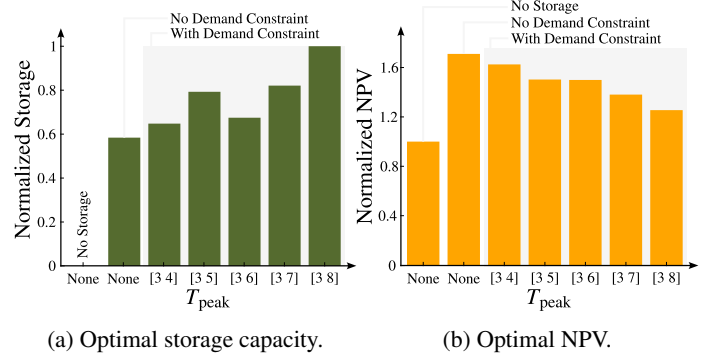


**FIGURE 7:** Case Study I: Sensitivity of normalized optimal storage capacity and net present value (NPV) objective function to the duration of the demand-following constraint for the natural gas combined cycle (NGCC) power plant with carbon capture and storage (CCS) and thermal energy storage (TES).

**TABLE 3:** Sensitivity of the optimal storage capacity and NPV objective function to variations in the duration of the demand-following constraint for Case Study I.

Scenario	Optimal Storage	Optimal NPV
No Storage with CCS	-	-6.3170
No demand constraint	237.5290	-1.8298
$T_{\text{peak}} \in [3 - 4]$ PM	263.5106	-2.3677
$T_{\text{peak}} \in [3 - 5]$ PM	322.4310	-3.1409
$T_{\text{peak}} \in [3 - 6]$ PM	274.4213	-3.1627
$T_{\text{peak}} \in [3 - 7]$ PM	333.8728	-3.9114
$T_{\text{peak}} \in [3 - 8]$ PM	406.8284	-4.7072

following periods. To facilitate comparisons, both NPV and storage capacity are normalized according to the optimal results with no demand-following constraint. The results from this study are tabulated in Tab. 3 and shown in Fig. 7. According to these results, it is clear that under the current assumptions (IES architecture, carbon tax, price signals, parameters, etc.), the optimal thermal energy storage capacity generally increases with increasing the demand-following duration, with the exception of the results from  $T_{\text{peak}} = [3 6]$ . The optimal NPV decreases with increasing the demand duration.

Two important conclusions can be made by analyzing the optimal system behavior: (i) In a more restricted market scenario characterized by the presence of demand-following constraints, the role of the thermal energy storage system becomes increasingly prominent. (ii) Operating in an increasingly restricted market often results in poor economic performance of the integrated energy system. As is evident from these studies, ECOGEN-CCD enables the optimal performance assessment of the integrated en-

ergy system, facilitating the decision-making process in early-stage design with consideration of different scenarios, policies, and requirements.

### 3.2 Case Study II: Wind Farm with Battery Energy Storage Units

In this case study, we consider an on-shore wind farm with a large plant footprint operating at 200 [MW] in the Great Plains region in combination with a 50 [MW] battery storage rate. The wind farm parameters are based on a case with 71 wind turbines, and a nominal capacity of  $p_{\text{rated}} = 2.8$  [MW], with a rotor diameter of  $D = 125$  [m] and a hub height of 90 [m] [22]. Variations in wind speed cause fluctuations in the power outputted to the grid, negatively affecting power quality and stability. Therefore, a BESS is needed to mitigate these adverse impacts [29]. Lithium-ion batteries offer high power density and energy efficiency, making them a promising energy storage technology for wind farm applications [30]. Therefore, a utility-scale lithium-ion battery consisting of 25 modular, prefabricated battery storage container buildings is considered here [22]. Further details about the parameters used here can be found in Ref. [22].

As opposed to Case Study I, where the operator can request a specific power output from the generator, the wind farm operation is primarily determined by the availability of wind. Using wind speed  $v_w(t)$  as an additional time-dependent input to the model, the upper bound of Eq. (11) was estimated for each turbine based on the wind speeds, wind farm specifications, and the capacity factor of  $c_p = 0.55$ :

$$p_w = c_p \frac{1}{2} \rho_{\text{air}} \frac{\pi D^2}{4} v_w(t)^3 \quad (30)$$

where  $p_w$  is the wind power, and  $\rho_{\text{air}}$  is the air density. The maximum wind power is assumed to happen at  $v_w = 25$  [m/s], and the turbine is off for wind speeds above this value. All of the power vector elements greater than  $p_{\text{rated}}$  are saturated at this value. Finally, the available power output takes into consideration the number of wind turbines in the farm. The input parameters associated with this case study are tabulated in Tables 1 and 4. The candidate system is illustrated in Fig. 2b, where the electrical load is present due to the need to operate auxiliary equipment in the facility (auxiliary loads).

Unlike in the previous case, the generator power level here is mainly determined by the availability of wind and wind turbine characteristics. Therefore, in Fig. 8a, the generator captures all the wind power that it is capable of harvesting. On the other hand, the charge and discharge decisions are heavily determined by the electricity prices. As it is clear from Fig. 8c, when the electricity prices are high, the charge signal decreases, and the discharge signal increases. This results in dramatic drops in the storage state, as evidenced by region ①, in Figs. 8b and 8c. Ideally, this outcome should increase the power sold to the grid and, thus, increase revenue. However, since the wind power avail-

**TABLE 4:** Parameters associated with Case Study II for a wind farm connected to a battery energy storage system, largely based on Ref. [22].

Field	Value	Unit	Field	Value	Unit
$\rho_{\text{fuel}}$	0	kg/h.MW	$\alpha_{\text{CO}_2}$	0	ton/kg
$\tau$	0	h	$\eta_G$	1	-
$u_{G,\text{min}}$	0	MW	$u_{G,\text{max}}$	200	MW
$x_{G,\text{min}}$	0	MW	$x_{G,\text{max}}$	200	MW
$x_S(t_0)$	15	MWh	$x_G(t_f)$	15	MWh
$\vec{u}_{\text{max}}$	50	MW	$\vec{u}_{\text{max}}$	50	MW
$L_P$	0	MW	$L_E$	$0.1x_G$	MW
$T_{\text{con}}$	5	years	$r$	0.075	-

able in this period is relatively lower than the neighboring time periods (see Fig. 8a), the power sold to the grid remains comparatively low. This is shown in Fig. 8d.

The optimal storage capacity is 92.45 [MWh], and the NPV objective function is  $\$ 0.69 \times 10^9$ , indicating that for a large wind farm, a utility-scale BESS has the potential to be economically competitive. The percentages associated with the energy produced by the generator and the shares of the generator and storage unit from the electrical load and revenue are shown in Fig. 9. Accordingly, 15.2% of the generated energy is used to charge the BESS, while 5.25% is used to satisfy the electric load demands. Over the project's life, the storage will satisfy 47.5% of this load demand, and the generator will satisfy the remainder. Finally, storage contributions to the revenue are estimated as 17.5%.

Among others, the solution presented here strongly depends on the arbitrarily-selected wind profile. The location of the farm, however, has a significant impact on its technical and economic performance [31]. To gain a deeper understanding of the impact of wind profile and its tight association with the location of the farm, we extend this study to assess the performance of the farm across various U.S. locations, using the average hourly wind data collected and maintained by the National Oceanic and Atmospheric Administration in Ref. [32]. While interval prediction can be used to predict wind power output scenarios [33], nominal average hourly values based on historical data are used here. The candidate locations for the wind farm are shown in Fig. 10a. The NPV objective function, along with the optimal sizing of the BESS at each location, is found and presented in Fig. 10b.

These investigations are performed in the presence of a multitude of assumptions, including fixed electricity prices across all states. From these figures, it is clear that wind farms located in Colorado (CO), New Mexico (NM), and Texas (TX) have a high potential for successful commercialization. These 3 site locations are characterized by high winds (and thus, high mean power output from the farm) with a small standard deviation in the generated wind power. The relatively high and constant availability

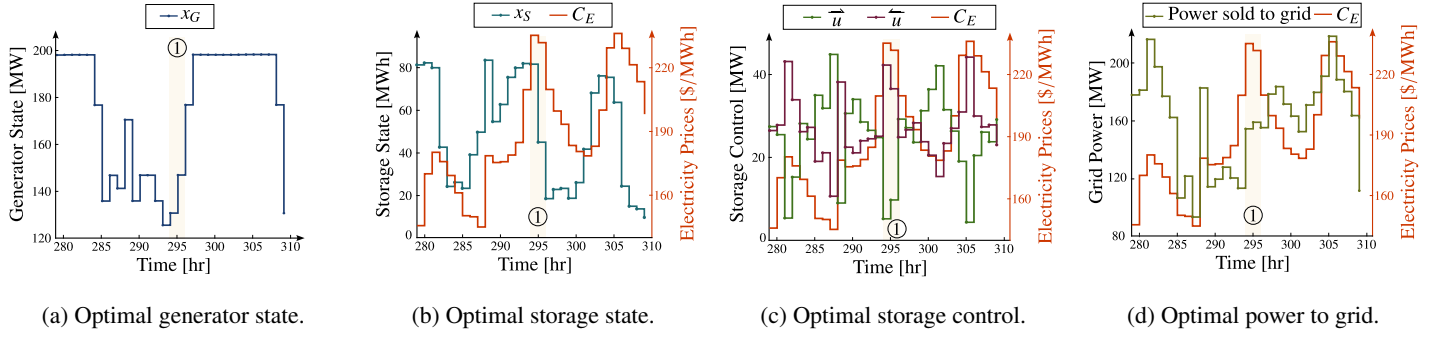


**FIGURE 8:** Case Study II: Optimal state and control variables for a wind farm with a battery storage unit.

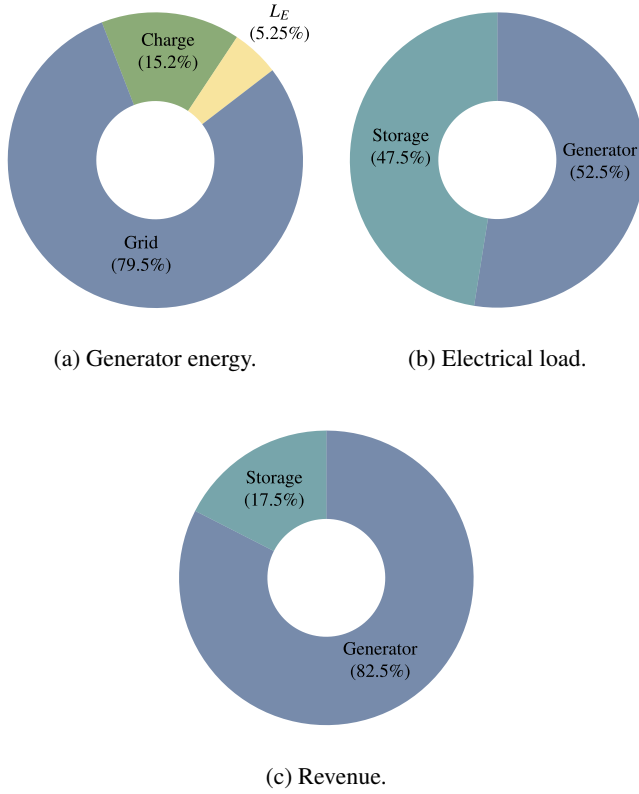


**FIGURE 9:** Breakdown of various elements in Case Study II, a wind farm with battery energy storage units: (a) Generator energy usage, (b) Electrical load contributions, and (c) Revenue contributions.

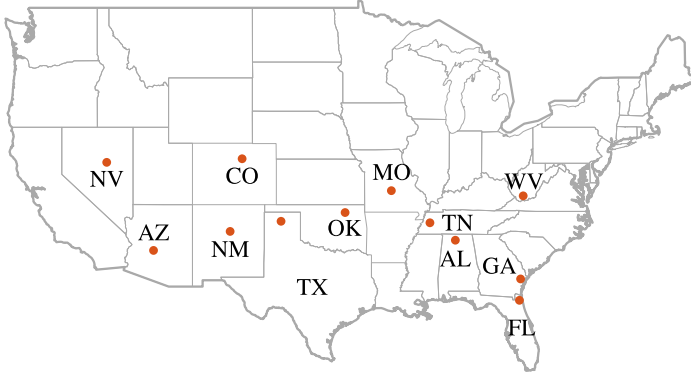
of wind energy in these regions informs the need for relatively small BESS under the considered electricity price signal. The largest optimal storage capacity belongs to Nevada (NV) and Alabama (AL). Both of these site locations are characterized by medium mean wind farm power and relatively high standard de-

viation. Note that while wind profile characteristics are determining factors in assessing the performance of the wind farm, their variation in relation to the electricity prices is the driver behind the optimal results presented here. Such complex interactions necessitate the need for an efficient optimization-based framework such as ECOGEN-CCD to inform optimal decision-making in defining crucial technical aspects of an IES.

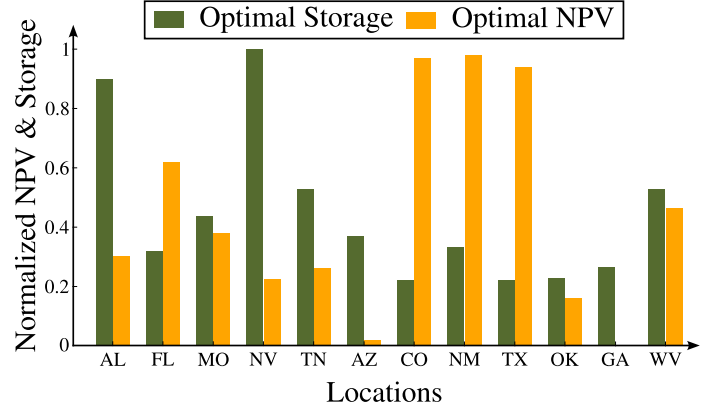
### 3.3 Nuclear Power Plant with Hydrogen Generation

Nuclear power plants (NPPs) play a crucial role in the future of the electricity market, as after hydropower, they are the largest energy source with low carbon emissions [34]. Nevertheless, their economic viability is challenged by low electricity prices from other generation sources, as well as other complexities. On the other hand, the hydrogen market has witnessed tremendous growth in the U.S. and globally, increasing more than threefold since 1975 [35]. The growing market for hydrogen signifies a unique opportunity for NPPs to expand into additional markets since the integration of NPPs with additional markets and technologies has the potential to keep NPPs competitive [3, 23, 36].

This case study considers the integration of NPP with a hydrogen facility and storage. This hybrid operation [23] releases NPPs from their traditional baseload by enabling them to strategically (based on economics) produce hydrogen or sell electricity to the grid. Here, we consider an NPP with two pressurized water reactors (PWR), in which the heat generated by the fuel in the reactor is released into the surrounding pressurized cooling water. The pressurized water absorbs the heat without boiling and, after passing through a steam generator, flows through a steam turbine to generate electricity. Hydrogen is produced via the high-temperature steam electrolysis (HTSE) process [37], which requires both thermal and electrical connections to NPP. Based on load requirements reported in Ref. [23], this study assumes that for every unit of electricity, 10% thermal energy is required to produce hydrogen. The thermal requirement is then defined as a function of the input electricity from the tertiary charging signal, effectively ensuring that the thermal loads are only present when a decision to produce hydrogen is made. The cost of the fuel



(a) Candidate farm locations.



(b) Optimal storage capacity and NPV.

**FIGURE 10:** Case Study II: Optimal storage capacity and NPV objective for the wind farm with a battery energy storage system (BESS) at various U.S. locations.

is constructed based on predictions presented in Ref. [38], while hydrogen market prices are assumed to be fixed at \$7.0 per kg of hydrogen, which is within the price range reported in Ref. [39]. The cost parameters for the NPP and the hydrogen generation and storage facility, which are largely based on Refs. [22, 23], are described in Tab. 1. The remaining problem parameters are shown in Tab. 5.

Informed by hydrogen market operations and the fact that sales of hydrogen can only occur at pre-scheduled times, this case study considers a discrete daily demand through the following constraint:

$$0 \leq u_{TR}(t) \leq \begin{cases} u_{\max}, & \text{if } t = 8 \text{ AM} \\ 0, & \text{otherwise} \end{cases} \quad (31)$$

According to this equation, hydrogen sales can only occur between 8 – 9 AM on a daily basis.

**TABLE 5:** Parameters associated with Case Study III for a nuclear power plant connected to a hydrogen production and storage facility, largely based on Refs. [22, 23, 36, 40, 41].

Field	Value	Unit	Field	Value	Unit
$\rho_{\text{fuel}}$	0.001	kg/h.MW	$\alpha_{\text{CO}_2}$	0	ton/kg
$\tau$	1.79	s	$\eta_G$	1	-
$u_{G,\min}$	0	MW	$u_{G,\max}$	2156	MW
$x_{G,\min}$	0	MW	$x_{G,\max}$	2156	MW
$x_S(t_0)$	500	kg	$x_G(t_f)$	500	kg
$\vec{u}_{\max}$	1065	MW	$\vec{u}_{\max}$	27990	kg/h
$L_P$	$0.1\vec{u}$	MW	$L_E$	$0.1x_G$	MW
$T_{\text{con}}$	7	years	$r$	0.075	-
$\alpha_{ET}$	0.0377	MWh/kg	$\alpha_{TE}$	29.762	kg/MWh

The problem is solved for 30 years of operation, and the results are presented in Fig. 11. According to Fig. 11a, the NPP power level drops significantly in region ①, where the electricity prices are low, and increases in region ② where electricity prices are high. As evidenced by Fig. 11b, during phase ① and ②, the level of hydrogen storage increases and decreases, respectively. According to Fig. 11c, direct sales of hydrogen, which become possible every day between 8 – 9 AM, results in a periodic discharge of hydrogen, in which the majority of the discharged hydrogen is directly sold to the market. The power sold to the grid is shown in Fig. 11d, where it is evident that the power sold to the grid is high in region ② when the electricity prices are high.

The optimal storage capacity is 15079 [kg], with the NPV objective function of  $-\$7.92 \times 10^9$ , indicating that under current assumptions, including retail prices, facility costs, and lifetime of the farm, the project needs further time to become profitable. Figure 12a indicates that from the total generator's energy, 72.04% was directly sold to the electricity grid, while 16% was used for charging the tertiary hydrogen storage, 10% used to satisfy auxiliary electrical loads, and 1.6% used to satisfy the primary load demand for HTSE. In this case study and with the presented assumptions, the storage is responsible for 7.29% of the generated revenue over the lifetime of the project. This result is shown in Fig. 12b.

According to Ref. [42], 60% to 70% of the cost of power produced by NPPs are directly related to capital costs. Since NPPs are characterized by large capital investments, the consideration of potential uncertainties in overnight construction costs ( $C_{\text{occ}}$ ) can inform project management, planning, and scheduling. It can also provide unique opportunities for understanding risks — informing further actions to protect investors [19]. The market prices for hydrogen, which are also inherently uncertain, have a significant impact on optimal system behavior and its eco-



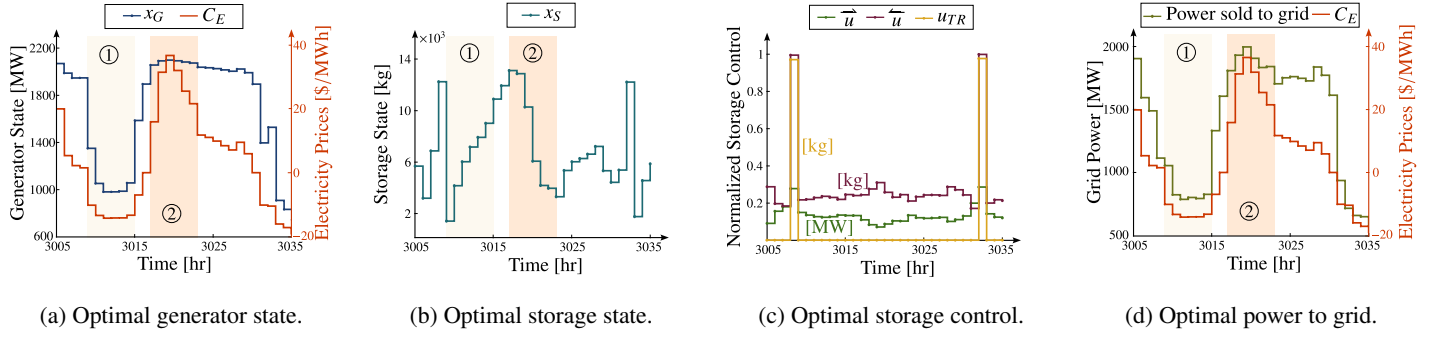


**FIGURE 11:** Case Study III: Optimal state and control variables for a nuclear power plant with a hydrogen production and storage facility.

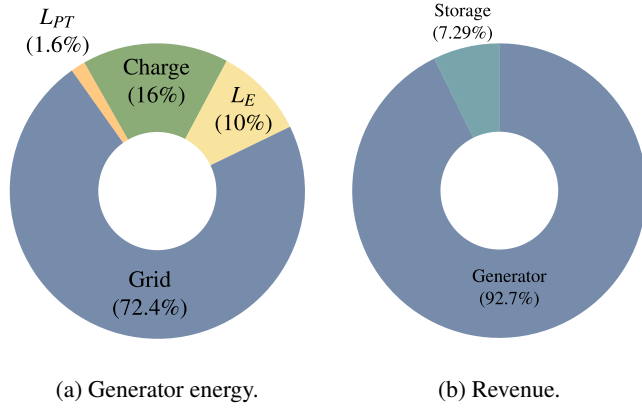


**FIGURE 12:** Breakdown of various elements in Case Study III, a nuclear power plant with hydrogen generation and storage facility: (a) Generator energy usage, and (b) Revenue contributions.

nomic performance. The impact of these uncertainties on the optimal performance of an NPP with hydrogen production and storage facility is explored next.

Here, we assume that the OCC associated with NPP is an uncertain variable defined within  $C_{OCC,NPP} \in [4000 \ 9000]$  [\$/kW] [19]. In addition, due to the significant impact of hydrogen market prices on optimal system behavior and its inherent uncertainties,  $C_T \in [3 \ 10]$  [\$/k] is also assumed to be an uncertain variable. In the following, we assess the impact of variations in  $C_{OCC}$  and hydrogen market prices on the optimal IES solution. Informed by the lack of data to construct the probability distribution, a crisp representation of uncertainties is used to characterize these uncertain quantities [43]. Various levels of overnight construction costs are then employed, along with various levels of hydrogen market prices, to construct surfaces for optimal NPV and storage capacity.

The results from these investigations are shown in Fig. 13. Specifically, Figs. 13a and 13b show variations in normalized optimal NPV and storage capacity when variations occur in both

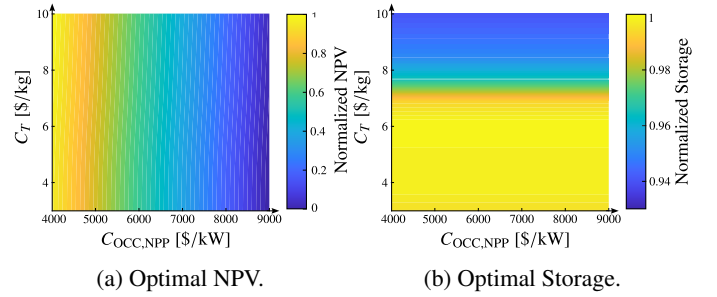


**FIGURE 13:** Case Study III: Optimal NPV and storage capacity for uncertainties in overnight construction cost of nuclear power plant and hydrogen market prices.

$C_{OCC,NPP}$  and  $C_T$ . From these results, it is clear that in the presence of uncertainties from OCC of the NPP and hydrogen market prices, the maximum NPV corresponds to the case with the lowest  $C_{OCC,NPP}$  and maximum  $C_T$ . This conclusion is shown in Fig. 13a. As shown in Fig. 13b, under the assumption of a prescribed generator capacity, the optima storage is independent of  $C_{OCC,NPP}$ ; however, it increases with lower hydrogen market prices.

## 4 CONCLUSION

In this article, we developed an efficient framework to assess the economic feasibility of integrated generator and storage energy systems. The proposed framework, referred to as ECOGEN-CCD, empowers the early-stage investigations of various concepts and configurations of integrated energy systems. It leverages a system-level, control co-design approach to identify the most profitable technology parameters and operations under specific assumptions. ECOGEN-CCD has the potential to offer unique insights for both new projects and retrofit efforts, facilitating the decision-making process and communications among technology experts, investors, and stakeholders.

The capabilities of ECOGEN-CCD were tested for three

case studies. Case Study I was focused on a power plant that includes a natural gas combined cycle generator, a thermal storage unit, and a carbon capture and storage system. Case Study II considered a wind farm with a battery storage system, thereby bringing up some of the complexities in dealing with non-dispatchable renewable technologies. Hybrid operation of a nuclear power plant with a hydrogen generation and storage facility was assessed in Case Study III. Since in its current form, ECOGEN-CCD solves a linear, convex optimization problem, the case studies were investigated for the duration of 30 years, on an hourly basis, in an efficient manner identifying the global optimal solution.

As a next step, it is desirable to enable the framework to account for the simultaneous presence of multiple storage types and other heterogeneous and more complex configurations. This framework, within its current and future capabilities, has the potential to further improve the economic viability of various integrated energy systems and the decision-making surrounding them.

## ACKNOWLEDGMENT

The authors would like to thank Ian Goven and Roberto Vercellino for their contributions to the development of this research.

## REFERENCES

- [1] Wu, J., Yan, J., Jia, H., Hatziargyriou, N., Djilali, N., and Sun, H., 2016. "Integrated energy systems". *Appl. Energy*, **167**, Apr., pp. 155–157. doi: [10.1016/j.apenergy.2016.02.075](https://doi.org/10.1016/j.apenergy.2016.02.075)
- [2] Berjawi, A., Walker, S., Patsios, C., and Hosseini, S., 2021. "An evaluation framework for future integrated energy systems: A whole energy systems approach". *Renew. Sustain. Energy Rev.*, **145**, July, p. 111163. doi: [10.1016/j.rser.2021.111163](https://doi.org/10.1016/j.rser.2021.111163)
- [3] Zhang, T., 2022. "Techno-economic analysis of a nuclear-wind hybrid system with hydrogen storage". *J. Energy Storage*, **46**, Feb., p. 103807. doi: [10.1016/j.est.2021.103807](https://doi.org/10.1016/j.est.2021.103807)
- [4] Arent, D. J., Bragg-Sitton, S. M., Miller, D. C., Tarka, T. J., Engel-Cox, J. A., Boardman, R. D., Balash, P. C., Ruth, M. F., Cox, J., and Garfield, D. J., 2021. "Multi-input, multi-output hybrid energy systems". *Joule*, **5**(1), Jan., pp. 47–58. doi: [10.1016/j.joule.2020.11.004](https://doi.org/10.1016/j.joule.2020.11.004)
- [5] HERON: Overview, a broad look at the holistic energy resource optimization network software. Tech. Rep. INL/MIS-22-66317, Idaho National Lab.
- [6] McDowell, D., Talbot, P., Wrobel, A., Frick, K., Bryan, H., Boyer, C., Boardman, R., Taber, J., and Hansen, J., 2021. A technical and economic assessment of LWR flexible operation for generation and demand balancing to optimize plant revenue. Tech. Rep. INL/EXT-21-65443-Revision-1, Idaho National Laboratory, Dec. doi: [10.2172/1844211](https://doi.org/10.2172/1844211)
- [7] Khamis, I., and Malshe, U., 2010. "HEEP: A new tool for the economic evaluation of hydrogen economy". *Int. J. Hydrog. Energy*, **35**(16), Aug., pp. 8398–8406. doi: [10.1016/j.ijhydene.2010.04.154](https://doi.org/10.1016/j.ijhydene.2010.04.154)
- [8] Garcia-Sanz, M., 2019. "Control co-design: An engineering game changer". *Adv. Control Appl.*, **1**(1), Oct. doi: [10.1002/adc2.18](https://doi.org/10.1002/adc2.18)
- [9] Vercellino, R., Markey, E., Limb, B. J., Pisciotto, M., Huyett, J., Garland, S., Bandhauer, T., Quinn, J. C., Psarras, P., and Herber, D. R., 2022. "Control co-design optimization of natural gas power plants with carbon capture and thermal storage". In International Design Engineering Technical Conferences. doi: [10.1115/detc2022-90021](https://doi.org/10.1115/detc2022-90021)
- [10] Soto Gonzalez, G., and Talbot, P., 2022. Force-dispatches integration - initial demonstration. Tech. Rep. INL/RPT-22-69033-Rev000; TRN: US2309045, Idaho National Laboratory, Sept. doi: [10.2172/1891636](https://doi.org/10.2172/1891636)
- [11] Li, B., Talbot, P., McDowell, D., and Hansen, J., 2021. Release a public version of HERON (HERON 2.0) with improved algorithms for the treatment of energy storage. Tech. Rep. INL/EXT-21-65473-Rev000; TRN: US2302624, Idaho National Lab, Dec. doi: [10.2172/1838610](https://doi.org/10.2172/1838610)
- [12] Herber, D. R., 2017. "Advances in combined architecture, plant, and control design". Ph.D. Dissertation, University of Illinois at Urbana-Champaign, Urbana, IL, USA, Dec.
- [13] DT QP project. <https://github.com/danielrherber/dt-qp-project>.
- [14] MIT Energy Initiative and Princeton University ZERO lab. GenX. <https://github.com/GenXProject/GenX>.
- [15] <https://github.com/AzadSaeed/ECOGEN-CCD/releases/tag/v1.0.0>.
- [16] Joskow, P. L., and Parsons, J. E., 2009. "The economic future of nuclear power". *Daedalus*, **138**(4), Sept., pp. 45–59. doi: [10.1162/daed.2009.138.4.45](https://doi.org/10.1162/daed.2009.138.4.45)
- [17] Mantripragada, H., and Rubin, E., 2018. "Techno-economic analysis methods for nuclear power plants". *SSRN*. doi: [10.2139/ssrn.3198421](https://doi.org/10.2139/ssrn.3198421)
- [18] International Atomic Energy Agency, 2013. Approaches for assessing the economic competitiveness of small and medium sized reactors. Tech. Rep. NP-T-3.7, Vienna.
- [19] Wealer, B., Bauer, S., Hirschhausen, C., Kemfert, C., and Göke, L., 2021. "Investing into third generation nuclear power plants - review of recent trends and analysis of future investments using monte carlo simulations". *Renew. Sustain. Energy Rev.*, **143**, June, p. 110836. doi: [10.1016/j.rser.2021.110836](https://doi.org/10.1016/j.rser.2021.110836)
- [20] Martins, J. R. R. A., and Ning, A., 2021. *Engineering Design Optimization*. Cambridge University Press, Nov. doi: [10.1017/9781108980647](https://doi.org/10.1017/9781108980647)
- [21] Herber, D. R., and Allison, J. T., 2017. "Unified scaling of dynamic optimization design formulations". In International Design Engineering Technical Conferences, American Society of Mechanical Engineers, p. V02AT03A003. doi: [10.1115/detc2017-67676](https://doi.org/10.1115/detc2017-67676)
- [22] U.S. Energy Information Administration, 2020. Capital cost and performance characteristic estimates for utility scale electric power generating technologies. Tech. rep.
- [23] Frick, K., Talbot, P., Wendt, D., Boardman, R., Rabiti, C., Bragg-Sitton, S., Ruth, M., Levie, D., Frew, B., Elgowainy, A., and Hawkins, T., 2019. Evaluation of hydrogen production feasibility for a light water reactor in the Midwest. Tech. Rep. INL/EXT-19-55395-Rev000; TRN: US2100362, Idaho National Lab, Sept. doi: [10.2172/1569271](https://doi.org/10.2172/1569271)
- [24] Rubin, E. S., and Zhai, H., 2012. "The cost of carbon capture and storage for natural gas combined cycle power plants". *Environ. Sci. Technol.*, **46**(6), Mar., pp. 3076–3084. doi: [10.1021/es204514f](https://doi.org/10.1021/es204514f)
- [25] Limb, B. J., Markey, E., Vercellino, R., Garland, S., Pisciotto, M., Psarras, P., Herber, D. R., Bandhauer, T., and Quinn, J. C., 2022. "Economic viability of using thermal energy storage for flexible carbon capture on natural gas power plants". *J. Energy Storage*, **55**, Nov., p. 105836. doi: [10.1016/j.est.2022.105836](https://doi.org/10.1016/j.est.2022.105836)
- [26] Grid status. <https://docs.gridstatus.io/en/latest/search.html>.
- [27] <https://www.eia.gov/dnav/ng/hist/rngwhhdm.htm>.
- [28] Jenkins, J. D., Chakrabarti, S., Cheng, F., and Neha, P., 2021. Summary report of the GenX and PowerGenome runs for generating price series (for ARPA-E FLECCS Project). doi: [10.5281/ZENODO.5765798](https://doi.org/10.5281/ZENODO.5765798)
- [29] Jannati, M., and Vahidi, B., 2024. "A master-slave adaptive linear neuron-based approach for cost-effective use of battery energy

storage systems in wind farms”. *Results Eng.*, **23**, p. 102410. doi: [10.1016/j.rineng.2024.102410](https://doi.org/10.1016/j.rineng.2024.102410)

- [30] Jiang, Q., Gong, Y., and Wang, H., 2013. “A battery energy storage system dual-layer control strategy for mitigating wind farm fluctuations”. *IEEE Trans. Power Syst.*, **28**(3), pp. 3263–3273. doi: [10.1109/TPWRS.2013.2244925](https://doi.org/10.1109/TPWRS.2013.2244925)
- [31] Azad, S., Herber, D. R., Khanal, S., and Jia, G., 2024. “Site-dependent solutions of wave energy converter farms with surrogate models, control co-design, and layout optimization”. In American Control Conference.
- [32] Palecki, M., Durre, I., Applequist, S., Arguez, A., and Lawrimore, J., 2021. U.S. climate normals 2020: U.S. hourly climate normals (1991–2020). Tech. rep., National Oceanic and Atmospheric Administration.
- [33] Luo, F., Meng, K., Dong, Z. Y., Zheng, Y., Chen, Y., and Wong, K. P., 2015. “Coordinated operational planning for wind farm with battery energy storage system”. *IEEE Trans. Sustain. Energy*, **6**(1), pp. 253–262. doi: [10.1109/TSTE.2014.2367550](https://doi.org/10.1109/TSTE.2014.2367550)
- [34] British Petroleum, 2016. Statistical review of world energy. <http://large.stanford.edu/courses/2016/ph240/stanchi2/docs/bp-2016.pdf>.
- [35] International Energy Agency, 2019. The future of hydrogen: Seizing today’s opportunities. <https://www.iea.org/reports/the-future-of-hydrogen>.
- [36] Hancock, S., and Westover, T., 2022. “Simulation of 15% and 50% thermal power dispatch to an industrial facility using a flexible generic full-scope pressurized water reactor plant simulator”. *Energies*, **15**(3), Feb., p. 1151. doi: [10.3390/en15031151](https://doi.org/10.3390/en15031151)
- [37] Mingyi, L., Bo, Y., Jingming, X., and Jing, C., 2008. “Thermodynamic analysis of the efficiency of high-temperature steam electrolysis system for hydrogen production”. *J. Power Sources*, **177**(2), Mar., pp. 493–499. doi: [10.1016/j.jpowsour.2007.11.019](https://doi.org/10.1016/j.jpowsour.2007.11.019)
- [38] Kryzia, D., and Gawlik, L., 2016. “Forecasting the price of uranium based on the costs of uranium deposits exploitation”. *Miner. Resour. Eng.*, **32**(3), Sept., pp. 93–110. doi: [10.1515/gospo-2016-0026](https://doi.org/10.1515/gospo-2016-0026)
- [39] Ramadan, M. M., Wang, Y., and Tooteja, P., 2022. “Analysis of hydrogen production costs across the united states and over the next 30 years”. arXiv:2206.10689
- [40] Settle, F. A., 2009. “Uranium to electricity: The chemistry of the nuclear fuel cycle”. *J. of Chem. Educ.*, **86**(3), Mar., p. 316. doi: [10.1021/ed086p316](https://doi.org/10.1021/ed086p316)
- [41] OECD and Nuclear Energy Agency, 2021. Technical and economic aspects of load following with nuclear power plants. Tech. rep. doi: [10.1787/29e7df00-en](https://doi.org/10.1787/29e7df00-en)
- [42] MacKerron, G., 1992. “Nuclear costs: Why do they keep rising?”. *Energy Policy*, **20**(7), pp. 641–652. doi: [10.1016/0301-4215\(92\)90006-N](https://doi.org/10.1016/0301-4215(92)90006-N)
- [43] Azad, S., and Herber, D. R., 2023. “An overview of uncertain control co-design formulations”. *J. Mech. Des.*, **145**(9), July. doi: [10.1115/1.4062753](https://doi.org/10.1115/1.4062753)

## 5 APPENDIX

This section includes some complementary information, providing more details for understanding the optimization model.

### A Node Definitions

Mathematical descriptions of the nodes labeled in Fig. 1 are presented in this section. These equations, which are used to formulate inequality constraints associated with Eqs. (14)–(15), present the available amount of power from the generator at different stages, are described in further detail in Tab. 6.

### B Optimization Model

The inputs into the optimization model, along with outputs consisting of the NPV objective function and optimized decision variables, are graphically illustrated in Fig. 14. Note that this description is representative, and depending on the problem at hand, more advanced technical and economic parameters may be included.

### C Lexical Interpretations of Problem Elements

This section serves as a complementary section to the mathematical explanations offered throughout the article. Specifically, in this section, we offer some lexical interpretations to facilitate the understanding of various problem elements by non-optimization experts. These interpretations are offered in Tab. 7.

## Nomenclature

### Acronyms

BESS	battery energy storage system
CCD	control co-design
CCS	carbon capture and storage
HES	hybrid energy systems
HTSE	high-temperature steam electrolysis
IES	integrated energy systems
LWR	light water reactor
NGCC	natural gas combined cycle
NPV	net present value
NPP	nuclear power plant
TES	thermal energy storage

### Subscripts

• <i>E</i>	index for electrical domain
• <i>G</i>	index for generator
• <i>P</i>	index for primary domain
• <i>S</i>	index for storage
• <i>T</i>	index for tertiary domain
• <i>R</i>	index for revenue

### Select Variables

$C_{\text{cap}}$	capital cost
$\text{CO}_2$	$\text{CO}_2$ penalty
$C_E$	electricity price signal
$C_{\text{fom}}$	fixed O&M cost
$C_{\text{fuel}}$	fuel price signal
$C_P$	primary price signal
$C_T$	tertiary price signal
$C_{\text{vom}}$	variable O&M cost
$E_{\text{fuel}}$	fuel expenditure
$L$	load
$n$	node
$R$	revenue
$r$	discount rate
$T_{\text{con}}$	construction time

$\mathbf{u}$	control vector	$\Sigma$	storage capacity
$\overrightarrow{u}$	charging signal	$\overrightarrow{\eta}$	charge efficiency
$\overleftarrow{u}$	discharging signal	$\overleftarrow{\eta}$	discharge efficiency
$\mathbf{x}$	state vector		

**TABLE 6:** Node signal definitions with lexical interpretation from Fig. 1.

Lexical interpretation	Mathematical description
Initial available primary-type power	$n_1 : x_G$
Available primary-type power after charging primary storage units	$n_2 : x_G - \overrightarrow{u}_P$
Available primary-type power after satisfying primary loads	$n_3 : x_G - \overrightarrow{u}_P - L_{GP}$
Available primary-type power after satisfying the primary load for tertiary operation	$n_4 : x_G - \overrightarrow{u}_P - L_{GP} - L_{GPT}$
Available electrical power after accounting for power conversion efficiency	$n_5 : \eta_G(x_G - \overrightarrow{u}_P - L_{GP} - L_{GPT})$
Available electrical power after charging electrical storage	$n_6 : \eta_G(x_G - \overrightarrow{u}_P - L_{GP} - L_{GPT}) - \overrightarrow{u}_E$
Available electrical power after satisfying electrical load	$n_7 : \eta_G(x_G - \overrightarrow{u}_P - L_{GP} - L_{GPT}) - \overrightarrow{u}_E - L_{GE}$
Available electrical power after satisfying electrical load for tertiary operation	$n_8 : \eta_G(x_G - \overrightarrow{u}_P - L_{GP} - L_{GPT}) - \overrightarrow{u}_E - L_{GE} - \overrightarrow{u}_T$
Available electrical power after combusting tertiary product	$n_9 : \eta_G(x_G - \overrightarrow{u}_P - L_{GP} - L_{GPT}) - \overrightarrow{u}_E - L_{GE} - \overrightarrow{u}_T + \alpha_c \overrightarrow{\eta}_T \overrightarrow{u}_T - \alpha_c \overrightarrow{\eta}_T u_{TR}$
Primary-type power supplied by the generator to satisfy the primary load demand	$L_{GP} = L_P x_G - \overrightarrow{\eta}_P \overrightarrow{u}_P + \overrightarrow{\eta}_P u_{PR}$
Primary-type power supplied by the generator to satisfy the primary load demand for tertiary operation	$L_{GPT} = L_{PT} \overrightarrow{u}_T$
Electrical power supplied by the generator to satisfy the electrical load demand	$L_{GE} = L_E x_G - \overrightarrow{\eta}_E \overrightarrow{u}_E + \overrightarrow{\eta}_E u_{ER}$

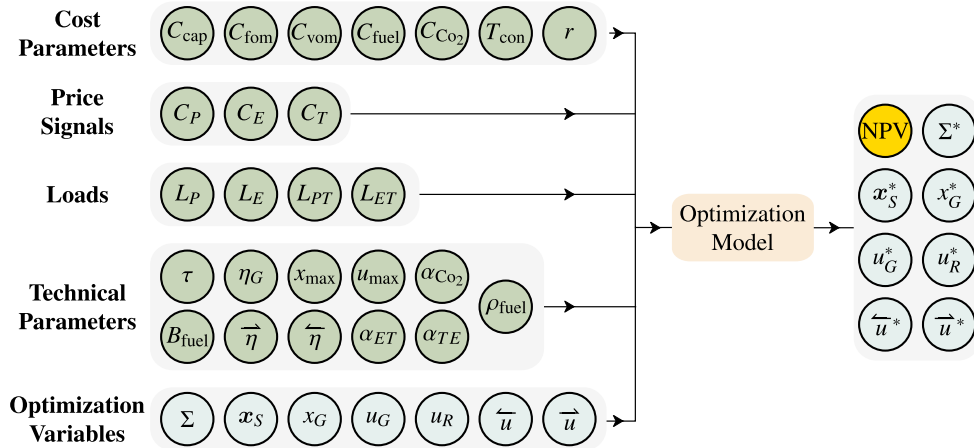


**FIGURE 14:** Optimization model with inputs and outputs.

**TABLE 7:** Lexical interpretation for select elements in the optimization problem.

Lexical interpretation	Mathematical description	Reference
The objective function is the <b>maximization</b> of the <b>Net Present Value</b> of the system over the lifetime of the power plant	maximize NPV	Eq. (16)
<b>Generator state dynamics</b> describes the power level of the generator unit as a function of <b>ramp rate</b> , generator's current state, and the requested power	$\dot{x}_G(t) = \frac{1}{\tau}(-x_G(t) + u_G(t))$	Eq. (5)
<b>Storage state dynamics</b> describes the available resource in the storage system as a function of <b>charging</b> and <b>discharging</b> power signals, and the storage <b>efficiencies</b>	$\dot{x}_S(t) = \overrightarrow{\eta} \overrightarrow{u}(t) - \overleftarrow{\eta} \overleftarrow{u}(t)$	Eq. (6)
<b>Storage capacity</b> must be <b>non-negative</b>	$0 \leq \Sigma$	Eq. (9)
At every time instant, control variables are <b>non-negative</b> and limited by a <b>maximum limit</b>	$0 \leq u(t) \leq u_{\max}$	Eq. (10)
Revenue control signal is never greater than the control <b>discharged power</b>	$u_{PR}(t) \leq \overleftarrow{u}_P(t)$ $u_{ER}(t) \leq \overleftarrow{u}_E(t)$ $u_{TR}(t) \leq \overleftarrow{u}_T(t)$	Eqs. (10b)–(10d)
The generator's power level is <b>non-negative</b> and limited by <b>nominal capacity</b> or <b>maximum available power to extract</b>	$x_{G,\min}(t) \leq x_G(t) \leq x_{G,\max}(t)$	Eq. (11)
The storage energy level is <b>non-negative</b> and never greater than the <b>storage capacity</b>	$0 \leq x_S(t) \leq \Sigma$	Eq. (12)
The generator and storage states are prescribed a <b>specific value</b> at $t_0$ and storage may also be prescribed <b>to the initial value</b> at $t_f$	$x(t_0) = x_0$ $x_S(t_f) = x_S(t_0)$	Eq. (13)
Each <b>charging</b> signal is limited by the <b>available power in the generator</b> at that node	$\overrightarrow{u}_P(t) \leq n_1(t)$ $\overrightarrow{u}_E(t) \leq n_5(t)$ $\overrightarrow{u}_T(t) \leq n_7(t)$	Eq. (14)
The generator's power signals to satisfy primary and electrical loads is <b>non-negative</b> and always smaller or equal to the <b>available power in the corresponding node</b>	$0 \leq L_{GP}(t) \leq n_2(t)$ $0 \leq L_{GPT}(t) \leq n_3(t)$ $0 \leq L_{GE}(t) \leq n_5(t)$	Eq. (15)